GEOPHYSICS, VOL. 84, NO. 5 (SEPTEMBER-OCTOBER 2019); P. S365–S372, 9 FIGS.
10.1190/GEO2018-0817.1

Data-driven internal multiple elimination and its consequences for imaging: A comparison of strategies

Lele Zhang[1], Jan Thorbecke[1], Kees Wapenaar[1], and Evert Slob[1]

ABSTRACT

We have compared three data-driven internal multiple reflection elimination schemes derived from the Marchenko equations and inverse scattering series (ISS). The two schemes derived from Marchenko equations are similar but use different truncation operators. The first scheme creates a new data set without internal multiple reflections. The second scheme does the same and compensates for transmission losses in the primary reflections. The scheme derived from ISS is equal to the result after the first iteration of the first Marchenko-based scheme. It can attenuate internal multiple reflections with residuals. We evaluate the success of these schemes with 2D numerical examples. It is shown that Marchenko-based data-driven schemes are relatively more robust for internal multiple reflection elimination at a higher computational cost.

INTRODUCTION

Creating an image of the subsurface from seismic reflection data is done by migration. Many migration schemes are based on the single-scattering assumption. This means that all events in the data are treated as single reflection events. Waves that have been reflected multiple times before being recorded are also migrated and end up as ghost reflectors in the migration image. In marine data, the free-surface-related multiple reflections can be very strong compared to the measured reflection response from the subsurface. These free-surface multiple reflections cause major ghost reflectors in the migration image. Several schemes have been developed to eliminate free-surface-related multiple reflections. The surface-related multiple-elimination (SRME) scheme of Verschuur et al. (1992) is a good example. SRME uses a minimum-energy criterion to eliminate the free-surface-related multiple reflections from the measured data. Besides free-surface multiples, there are internal multiple reflections that also introduce ghost reflectors in the migration image. These internal multiple reflections can be strong in land and marine seismic data, and most schemes fail to remove them from the measured reflection response.

A method that relies on the discrimination of moveout between primary and internal multiple reflections is proposed by Hampson (1986). Unfortunately, it is difficult to distinguish the moveout velocities of internal multiple reflections from those of primary reflections in most cases. Berkhout and Verschuur (1997) propose to attenuate internal multiple reflections by a layer-stripping scheme, in which a velocity model is needed to create redatumed data. Jakubowicz (1998) proposes to combine three primary reflections to predict and attenuate the first-order internal multiple reflections. However, these primary reflections need to be identified and picked from the measured reflection response. The inverse scattering series (ISS)-based internal multiple reflection attenuation scheme, proposed by Weglein et al. (1997), can be used to predict all orders of internal multiple reflections with approximate amplitudes in one step without model information (Ten Kroode, 2002; Löer et al., 2016). A global or local matching filter is usually required to subtract the predicted internal multiple reflections from the measured reflection response (Matson et al., 1999; Luo et al., 2011; de Melo et al., 2014).

Recently, Marchenko imaging (Broggini and Snieder, 2012; Slob et al., 2014; Wapenaar et al., 2014) has been proposed to image the subsurface without artifacts due to internal multiple reflections. This can be seen as a migration scheme that avoids migrating internal multiple reflections. Singh et al. (2015, 2017) extend the Marchenko imaging scheme to also account for free-surface-related multiple reflections, such that the free-surface and internal multiple reflections do not end up in the migration image. Ravasi (2017) modifies the scheme of Singh et al. (2017) for marine seismic data and shows the performance in numerical and field examples. Meles et al. (2016) retrieve a data set containing approximately only

Manuscript received by the Editor 22 November 2018; revised manuscript received 1 March 2019; published ahead of production 21 June 2019; published online 08 August 2019.
[1]Delft University of Technology, 2628 CN Delft, The Netherlands. E-mail: l.zhang-1@tudelft.nl (corresponding author); j.w.thorbecke@tudelft.nl; c.p.a.wapenaar@tudelft.nl; e.c.slob@tudelft.nl.

primary reflections by combining the Marchenko scheme with convolutional interferometry. To solve the Marchenko equations, we require the first arrival of the focusing wavefield estimated from a macrovelocity model. Van der Neut and Wapenaar (2016) propose a data-driven scheme for adaptive overburden elimination. This scheme can be used to eliminate the internal multiple reflections from the measured reflection response. It is derived from the coupled Marchenko equations by projecting the focusing points back to the acquisition surface. In their implementation velocity model, information is needed to create time truncations. The scheme has been modified and illustrated with 2D numerical examples (Zhang and Staring, 2018). Zhang et al. (2019) derive a new scheme from the revised coupled Marchenko equations (Zhang et al., 2018) to eliminate internal multiple reflections and compensate for transmission losses contained in primary reflections. They remove the need for model information by adapting the chosen depth level to an unknown variable depth such that the truncation time is constant for all offsets. The performance of this scheme has been illustrated with 2D numerical examples and the extension to account for free-surface multiple reflections has been achieved (Zhang and Slob, 2019) as well. Because the truncation choices made in Zhang et al. (2019) can be used in the scheme of van der Neut and Wapenaar (2016), both schemes can eliminate internal multiple reflections without any model information.

In this paper, we compare the data-driven schemes derived from coupled Marchenko equations (van der Neut and Wapenaar, 2016; Zhang et al., 2019) and from ISS (Ten Kroode, 2002; Löer et al., 2016). For the ISS-based internal multiple attenuation scheme derived by Weglein et al. (1997), it works in a space and in a background medium, and there is no comparative relation with Marchenko-based schemes. Thus, it is not included in this paper for the comparison. The comparison covers the theory and the performance in numerical examples. The paper is organized as follows. In the "Theory" section, we analyze the relation and difference among the three schemes. In the numerical section, we apply these schemes to simple and complex 2D numerical examples, compare their performance, and investigate the consequence on the migrated image. The advantages and disadvantages of these schemes are discussed, and we end with our conclusions.

THEORY

To clarify our notation, we indicate time as t and spatial location as $\mathbf{x} = (\mathbf{x}_H, z)$, where $\mathbf{x}_H$ denotes the horizontal coordinates (x and y) and z denotes the depth. We assume the medium to be lossless. The acoustic impulse reflection response is expressed as $R(\mathbf{x}_0', \mathbf{x}_0, t)$, where $\mathbf{x}_0$ denotes the source position and $\mathbf{x}_0'$ denotes the receiver position at the boundary $\partial\mathbf{D}_0$. The acoustically transparent acquisition boundary $\partial\mathbf{D}_0$ is defined at $z = 0$. In this section, the equations for the three schemes are given and briefly discussed.

Marchenko multiple elimination

As presented by van der Neut and Wapenaar (2016), the Marchenko multiple-elimination (MME) scheme is derived from the coupled Marchenko equations by projecting the focusing functions for all focusing points at a particular depth level back to a receiver location at the acquisition surface. The details of the derivation can be found in van der Neut and Wapenaar (2016). The scheme can be formulized as

$$R_t(\mathbf{x}_0', \mathbf{x}_0'', t) = R(\mathbf{x}_0', \mathbf{x}_0'', t) + \sum_{m=1}^{\infty} M_m(\mathbf{x}_0', \mathbf{x}_0'', t) \quad (1)$$

with

$$M_m(\mathbf{x}_0', \mathbf{x}_0'', t) = (\mathbf{R}\Theta_\tau^{t-\tau}\mathbf{R}^*\Theta_\tau^{t-\tau})M_{m-1}(\mathbf{x}_0', \mathbf{x}_0'', t), \quad (2)$$

and

$$M_0 = R, \quad (3)$$

where $\mathbf{R}$ indicates an integral operator of the measured reflection data R convolved with any wavefield and $\mathbf{R}^*$ is a correlation integral operator. The term $\Theta_\tau^{t-\tau}$ is the truncation operator to exclude values outside of the window $(\tau, t-\tau)$, M_m with $m = 1, \ldots, \infty$ give all orders of predicted internal multiple reflections, R_t denotes the retrieved primary reflections, and τ indicates the half-wavelength of the source wavelet to account for the finite bandwidth of the measured reflection response. Equation 3 is the start of this recurrent scheme presented in equations 1 and 2. The integral form of M_m can be written as

$$\begin{aligned} &M_m(\mathbf{x}_0', \mathbf{x}_0'', t) \\ &= \int_0^{+\infty} dt' \int_{\partial\mathbf{D}_0} d\mathbf{x}_0''' R(\mathbf{x}_0', \mathbf{x}_0''', t') H(t - t' - \tau) \\ &\quad \times \int_0^{+\infty} dt'' \int_{\partial\mathbf{D}_0} d\mathbf{x}_0 R(\mathbf{x}_0''', \mathbf{x}_0, t'') H(t' - t'' - \tau) \\ &\quad \times M_{m-1}(\mathbf{x}_0, \mathbf{x}_0'', t - t' + t''), \end{aligned} \quad (4)$$

where H indicates the Heaviside function to impose the truncation. As discussed by van der Neut and Wapenaar (2016), $M_1 = \mathbf{R}\Theta_\tau^{t-\tau}\mathbf{R}^*\Theta_\tau^{t-\tau}R$ can be used to predict all orders of internal multiple reflections at once with the wrong amplitude. The following updates $(M_2, \ldots, M_\infty)$ from the second term in equation 1 converge to the correct amplitude of internal multiple reflections predicted by M_1. The projected Marchenko equations from van der Neut and Wapenaar (2016) remove the initial downgoing focusing function from the scheme. We further remove the need for model information by introducing the truncation time as an independent variable (Zhang et al., 2019). Now, the scheme is model-free.

Only primary reflections end up in R_t in equation 1. The first term in the right side of equation 1 is the original reflection data with internal multiple reflections. Consequently, the second term in the right side of equation 1 can be seen as an operator expression for eliminating internal multiple reflections in the original reflection data. It uses only the single-sided reflection response R and an offset independent time truncation $\Theta_\tau^{t-\tau}$. Therefore, it can be stated that equation 1 presents a totally data-driven scheme that can be used for eliminating the internal multiple reflections in the measured reflection response without any model information.

Transmission compensated Marchenko multiple elimination

Zhang et al. (2019) present the transmission-compensated Marchenko multiple-elimination (T-MME) scheme for eliminating internal multiple reflections and applying transmission loss compensation to the primary reflections. It is derived from the coupled Marchenko equations with a revised truncation operator. The detailed derivation can be found in Zhang et al. (2019). The scheme can be formulized as

$$R_r(\mathbf{x}_0', \mathbf{x}_0'', t) = R(\mathbf{x}_0', \mathbf{x}_0'', t) + \sum_{m=1}^{\infty} \bar{M}_m(\mathbf{x}_0', \mathbf{x}_0'', t) \tag{5}$$

with

$$\bar{M}_m(\mathbf{x}_0', \mathbf{x}_0'', t) = (\Theta_\tau^{t+\tau}\mathbf{R}\Theta_\tau^{t+\tau}\mathbf{R}^*)\bar{M}_{m-1}(\mathbf{x}_0', \mathbf{x}_0'', t), \tag{6}$$

and

$$\bar{M}_0 = R, \tag{7}$$

where R_r denotes the transmission loss compensated primary reflections and $\Theta_\tau^{t+\tau}$ is a new truncation operator to exclude values outside of the window $(\tau, t+\tau)$. Equation 7 is the start of this recurrent scheme presented in equations 5 and 6. Note that $\bar{M}_1$ already gives all orders of internal multiple reflections and transmission losses in primary reflections with the wrong amplitude. The higher order terms $\bar{M}_m$ with $m = 2, \ldots, \infty$ serve to balance the amplitude of events predicted by $\bar{M}_1$. The integral form of $\bar{M}_m$ can be given as

$$\begin{aligned}
&\bar{M}_m(\mathbf{x}_0', \mathbf{x}_0'', t) \\
&= \int_0^{+\infty} dt' \int_{\partial \mathbf{D}_0} d\mathbf{x}_0''' R(\mathbf{x}_0', \mathbf{x}_0''', t') H(t - t' + \tau) \\
&\times \int_0^{+\infty} dt'' \int_{\partial \mathbf{D}_0} d\mathbf{x}_0 R(\mathbf{x}_0''', \mathbf{x}_0, t'') H(t' - t'' + \tau) \\
&\times \bar{M}_{m-1}(\mathbf{x}_0, \mathbf{x}_0'', t - t' + t'').
\end{aligned} \tag{8}$$

Note that equation 8 is the same as equation 4 except for the Heaviside function that imposes the truncation. Here, we also adapt the chosen depth level to an unknown variable depth such that the truncation time $(\tau, t+\tau)$ is constant for all offsets and the new truncation operator is model-free.

The left side R_r in equation 5, that is using this different truncation in time, has transmission loss compensated primary reflections. The first term in the right side of equation 5 is the original reflection data with internal multiple reflections and transmission losses in primary reflections. The second term in the right side of equation 5 works as an operator for eliminating internal multiple reflections and compensating for transmission losses in the primary reflections. It is also a totally data-driven scheme. Note that T-MME scheme presented in equation 5 is similar to MME scheme presented in equation 1 with different truncation operators. The truncation operator $\Theta_\tau^{t-\tau}$ in MME gives the result in which internal multiple reflections are eliminated without touching primary reflections. The revised truncation operator $\Theta_\tau^{t+\tau}$ in T-MME not only eliminates internal multiple reflections but also compensates for transmission losses in the primary reflections. A detailed explanation can be found in Zhang et al. (2019).

Ten Kroode and Löer internal multiple attenuation

The scheme derived from the third term of ISS by Ten Kroode (2002) and Löer et al. (2016) can also predict internal multiple reflections. In this scheme, the reflection data are correlated twice with particular truncations. It can be formulized as (Löer et al., 2016)

$$\begin{aligned}
&M_{\mathrm{TKL}}(\mathbf{x}_0', \mathbf{x}_0'', t) \\
&= \int_0^{+\infty} dt' \int_{\partial \mathbf{D}_0} d\mathbf{x}_0''' R(\mathbf{x}_0', \mathbf{x}_0''', t') H(t - t' - \tau) \\
&\times \int_0^{+\infty} dt'' \int_{\partial \mathbf{D}_0} d\mathbf{x}_0 R(\mathbf{x}_0''', \mathbf{x}_0, t'') H(t' - t'' - \tau) \\
&\times R(\mathbf{x}_0, \mathbf{x}_0'', t - t' + t''),
\end{aligned} \tag{9}$$

where M_{TKL} indicates the prediction of all orders of internal multiple reflections like M_1 in equation 4. Please note that equation 9 is slightly different from the equation in Löer et al. (2016) because we use a different normalization and replace ε_1 and ε_2 by the half-wavelength of the source wavelet τ here. The Ten Kroode and Löer internal multiple-attenuation (TKL) scheme can be given as

$$R_t'(\mathbf{x}_0', \mathbf{x}_0'', t) = R(\mathbf{x}_0', \mathbf{x}_0'', t) + M_{\mathrm{TKL}}(\mathbf{x}_0', \mathbf{x}_0'', t), \tag{10}$$

where R_t' indicates the retrieved data.

Equation 9 is exactly the same as equation 4 with $m = 1$. It means that all orders of internal multiple reflections can be predicted at once with the wrong amplitude in equation 9. The retrieved data R_t' in equation 10 contain primary reflections and residuals of internal multiple reflections. Thus, the TKL scheme can be seen as an internal multiple reflection attenuation scheme.

EXAMPLES

In this section, two numerical examples are given to validate the effectiveness and to clarify the difference between the three schemes. In the two numerical examples, sources and receivers are positioned at the top of a model, and a Ricker wavelet with 20 Hz center frequency is emitted by the sources. The spacing of the sources and receivers is 5 m in the first numerical example and 12.5 m in the second one. The reflection response is modeled using a finite-difference scheme (Thorbecke and Draganov, 2011). Absorbing boundary conditions are applied around the models, and the direct wave has been removed from the modeled data. The correct velocity model is used to migrate the original and retrieved data sets for a best-case scenario in the second example subsection.

Horizontally layered example

In this subsection, we consider a model in which most reflectors are "invisible" to test the performance of the three schemes. This model is a horizontally layered model with constant velocity (1000 m/s) and constant layer thickness (100 m); only the density in the different layers varies as shown in Figure 1. The values of density are given as 1000, 2000, 300, 702, 412, 594, 457, 553,

481, 533, 494, 523, and 501 kg/m^3. The interesting point is that because of the parameters of this model, the primary reflection of the third reflector cancels the first internal multiple reflection between the first two reflectors. The third reflector causes a new multiple, which is canceled by the primary reflection from the fourth reflector, and so on. Hence, from the third reflector onward, the model is invisible in the reflection response. The reflection responses are computed for 601 shot gathers with 601 traces per gather. One of the computed shot gathers is shown in Figure 2a. Note that, indeed, only the primary reflections from the first two reflectors are visible. Figure 2b–2d shows the results obtained with MME (equation 1), T-MME (equation 5), and TKL (equation 10), respectively. It is important to note that in the data set retrieved by MME and T-MME (shown in Figure 2b and 2c), primary reflections due to deeper reflectors are perfectly recovered because of the elimination of the corresponding internal multiple reflections. However, in the data set retrieved by TKL, only the primary reflection due to the third reflector is recovered. This is caused by the fact that the TKL scheme can only successfully predict the internal multiple reflection between the first two reflectors in this case. Figure 2e gives the modeled primary reflections without transmission loss, which will be used as a reference to illustrate the success of T-MME for transmission loss compensation in primary reflections. We pick the zero-offset traces from the original, modeled primary reflections, and retrieved data sets and show them in Figure 3. All traces have been normalized by the same factor. Displayed in Figure 3a are the zero-offset traces from the original shot gather (OR) and the retrieved data set (IR) shown in Figure 2b. It can be seen that later arriving primary reflections have been successfully recovered. Figure 3b shows the zero-offset traces from modeled primary reflections (MD) shown in Figure 2e and the retrieved data set (IT) shown in Figure 2c. Note that the retrieved data by T-MME match well with the modeled primary reflections without transmission loss (quantitatively, approximately 4% error in the amplitude in the retrieved primary reflections). The comparison of zero-offset traces from original shot gather (OR) and retrieved data set

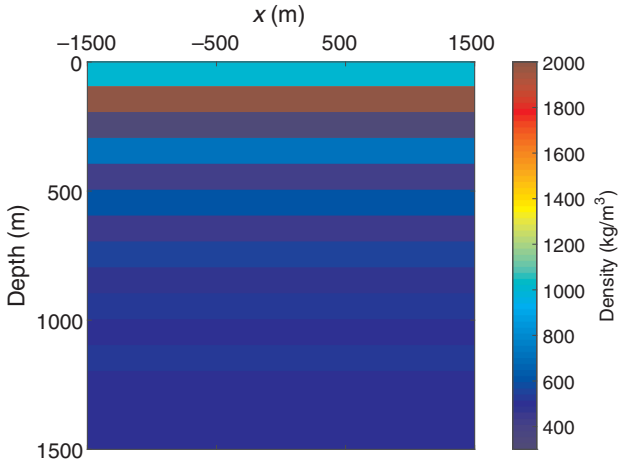

Figure 1. The density values of the invisible model.

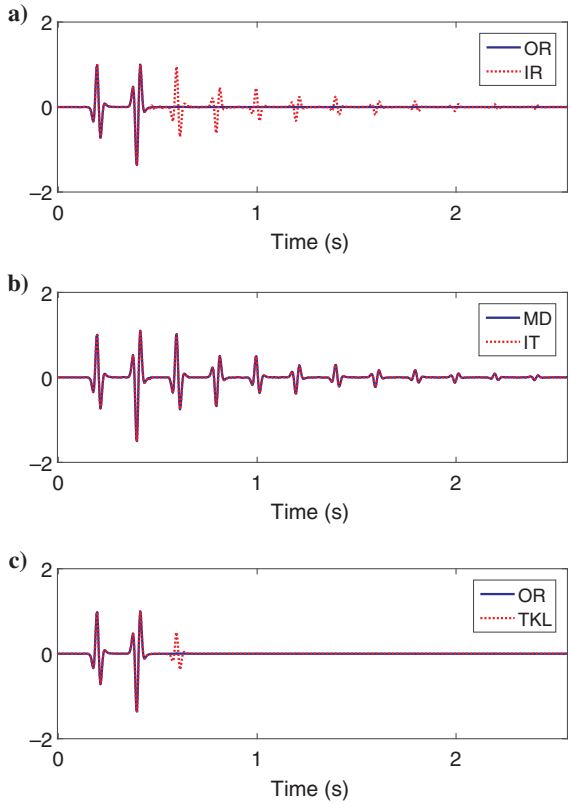

Figure 3. (a) A comparison of zero-offset traces from original and retrieved data sets shown in Figure 2a and 2b, (b) a comparison of zero-offset traces from modeled primary reflections and retrieved data sets shown in Figure 2e and 2c, and (c) a comparison of zero-offset traces from the original and retrieved data sets shown in Figure 2a and 2d.

Figure 2. (a) The modeled shot gather, (b) the data set retrieved by MME scheme with $m = 1, \ldots, 50$, (c) the data set retrieved by the T-MME scheme with $m = 1, \ldots, 50$, (d) the data set retrieved by the TKL scheme, and (e) the modeled primary reflections without transmission losses.

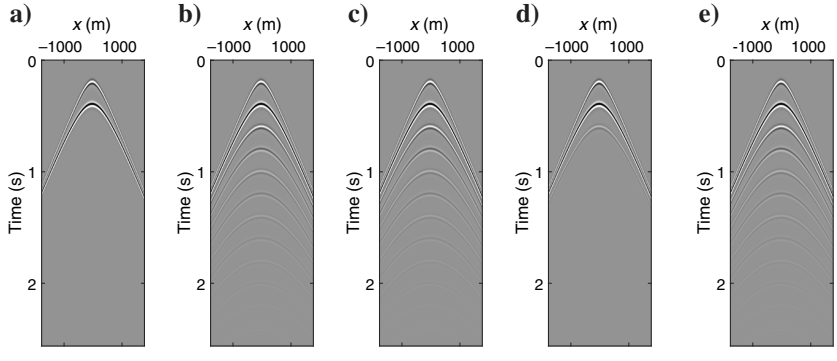

(TKL) shown in Figure 2d is given in Figure 3c. We can see that, although the third primary reflection has been recovered, the amplitude is relatively low compared with the results shown in Figure 3a and 3b. A similar conclusion can be derived from Figure 4 in which the comparison of nonzero-offset traces is given.

Complex medium example

Here, we show results from data computed in a complex model to test the performance of these schemes. Figure 5a and 5b shows the velocity and density values of this model. The reflection responses are computed for 480 shot gathers with 480 traces per gather. One of the computed shot gathers is shown in Figure 6a. Internal multiple reflections are present at later arrival times, and some of them are indicated by red arrows. The computed reflection responses are used as inputs to solve equations 1, 5, and 10, respectively. The resulting data sets are shown in Figure 6b–6d. The data retrieved by MME and T-MME are nearly multiple-free, and residuals of internal multiple reflections are present in the data retrieved by TKL. Detailed comparisons of amplitudes using zero-offset traces are given in Figure 7. All traces have been normalized by the same normalization factor. It can be seen in Figure 7a that the MME scheme can successfully eliminate internal multiple reflections without touching primary reflections. Figure 7b shows that the T-MME scheme eliminates internal multiple reflections and compensates for transmission losses in primary reflections. Figure 7c shows that the TKL scheme can attenuate internal multiple reflections with residuals present in the resulting data set and without touching the primary reflections. A similar conclusion can be derived from Figure 8 in which a comparison of nonzero-offset traces is given.

We use the computed and retrieved data sets to image the medium. The images obtained using a one-way wave-equation migration scheme are shown in Figure 9. We can see that in the images retrieved from the computed reflection responses and resulting data set of TKL, artifacts arising from internal multiple reflections are present. The images retrieved from the resulting data sets of MME and T-MME clearly show the primary reflectors without strong artifacts due to internal multiple reflections.

DISCUSSION

The simple and complex numerical examples show that all orders of internal multiple reflections can be eliminated by MME and T-MME if a sufficient number of updates are evaluated. Moreover, the T-MME scheme compensates for the transmission losses in the primary reflections such that the retrieved primary reflections have a higher amplitude as explained in Zhang et al. (2019). Unfortunately,

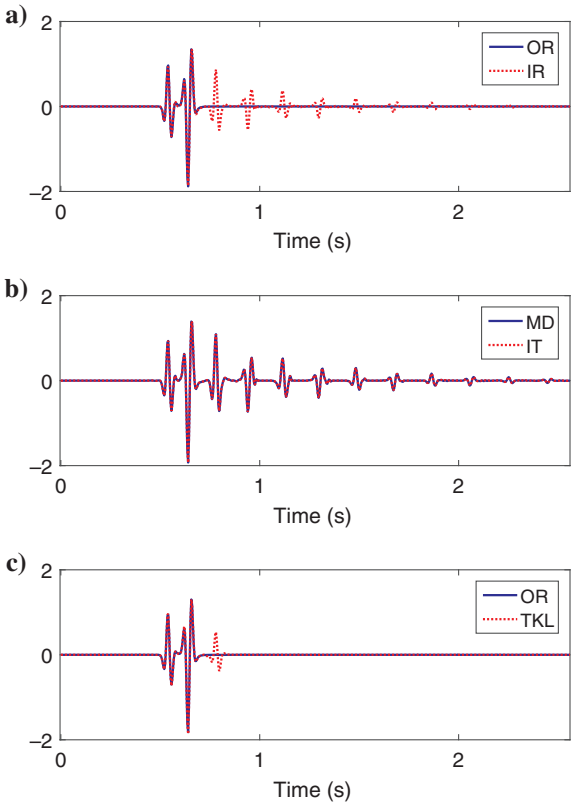

Figure 4. (a) A comparison of non-zero-offset (800 m) traces from the original and retrieved data sets shown in Figure 2a and 2b, (b) a comparison of nonzero-offset (800 m) traces from the modeled primary reflections and retrieved data sets shown in Figure 2e and 2c, and (c) a comparison of nonzero-offset (800 m) traces from the original and retrieved data sets shown in Figure 2a and 2d.

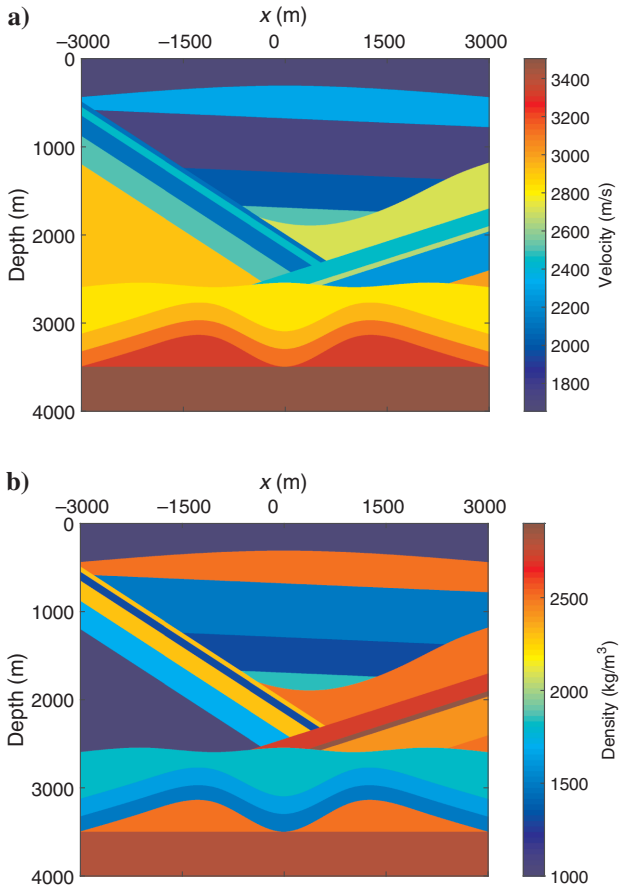

Figure 5. (a) The velocity and (b) density values of the complex model.

some limitations are still there. In the derivation of these two schemes, we assume that the medium to be lossless and the source wavelet to be known. These limitations will be the same for TKL because TKL can be understood as a partial solution of MME as we analyzed in the "Theory" section.

The TKL scheme estimates all orders of internal multiple reflections with wrong amplitude such that the data set retrieved in equation 10 contains residuals of internal multiple reflections. In the complex numerical example (as shown in Figure 9d), artifacts arising from migrated residuals of internal multiple reflections are strong enough to cause erroneous interpretation. To overcome this drawback, a global or local matching filter is usually used to subtract the predicted internal multiple reflections from the measured reflection response (Matson et al., 1999; Luo et al., 2011; de Melo et al., 2014). However, the subtracting filter cannot distinguish internal multiple reflections from primary reflections when they are overlapping each other, such that both of them are removed by the filter. The MME and T-MME would also suffer from this problem in a field case, in which imperfect deconvolution of the source wavelet and appearance of noise would cause erroneous amplitudes of predicted internal multiple reflections. Thus, for field data, a matching filter would be required for the subtraction of predicted internal multiple reflections from the measured data.

Note that, to analyze the relation and clarify the difference between schemes derived from Marchenko equations and ISS, the MME and T-MME schemes are presented as Neumann series expansions. In these expressions, we can recognize that the TKL scheme can be understood as the first iteration result of MME. However, the

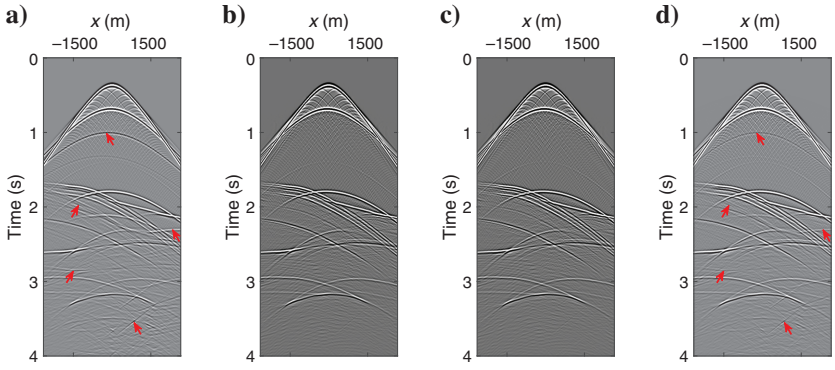

Figure 6. (a) Modeled shot gather, (b) the data set retrieved by MME scheme with $m = 1, \ldots, 20$, (c) the data set retrieved by the T-MME scheme with $m = 1, \ldots, 20$, and (d) the data set retrieved by the TKL scheme. The red arrows in (a) indicate the internal multiple reflections, and the red arrows in (d) indicate the residuals of the internal multiple reflections.

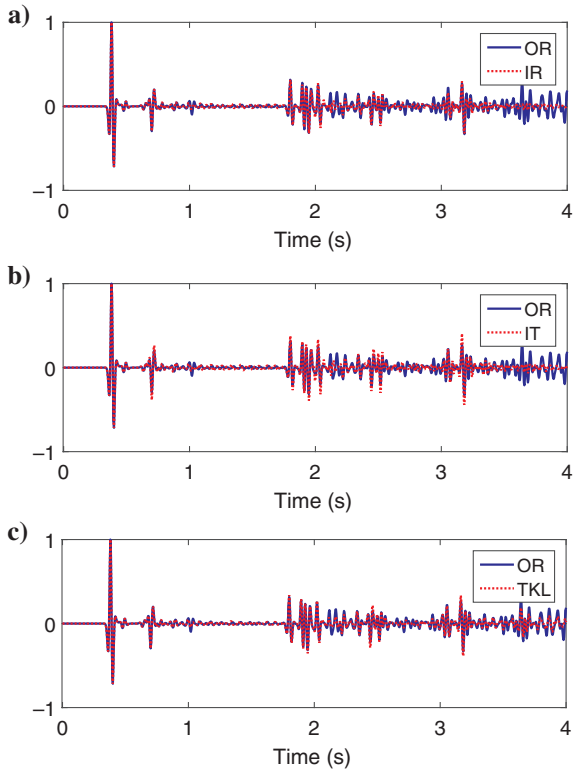

Figure 7. (a) A comparison of zero-offset traces from the original and retrieved data sets shown in Figure 6a and 6b, (b) a comparison of zero-offset traces from original and retrieved data sets shown in Figure 6a and 6c, and (c) a comparison of zero-offset traces from original and retrieved data sets shown in Figure 6a and 6d.

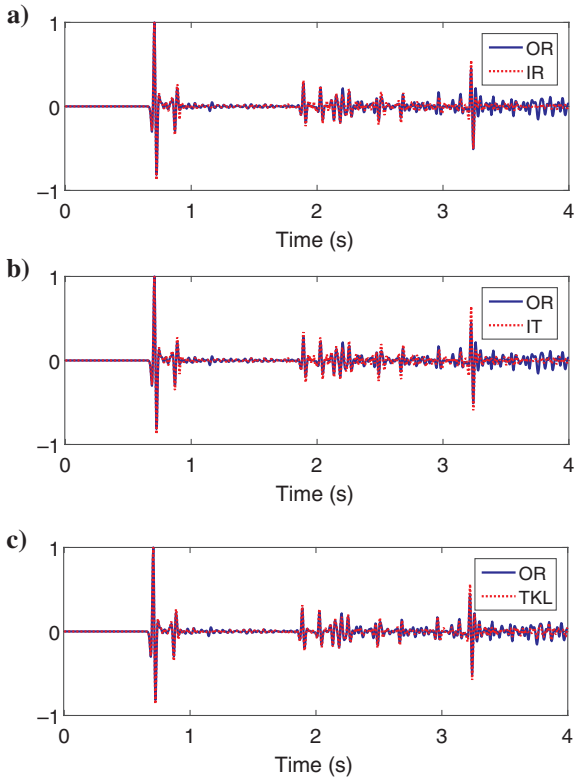

Figure 8. (a) A comparison of nonzero-offset (1000 m) traces from the original and retrieved data sets shown in Figure 6a and 6b, (b) a comparison of nonzero-offset (1000 m) traces from the original and retrieved data sets shown in Figure 6a and 6c, and (c) a comparison of nonzero-offset traces from the original and retrieved data sets shown in Figure 6a and 6d.

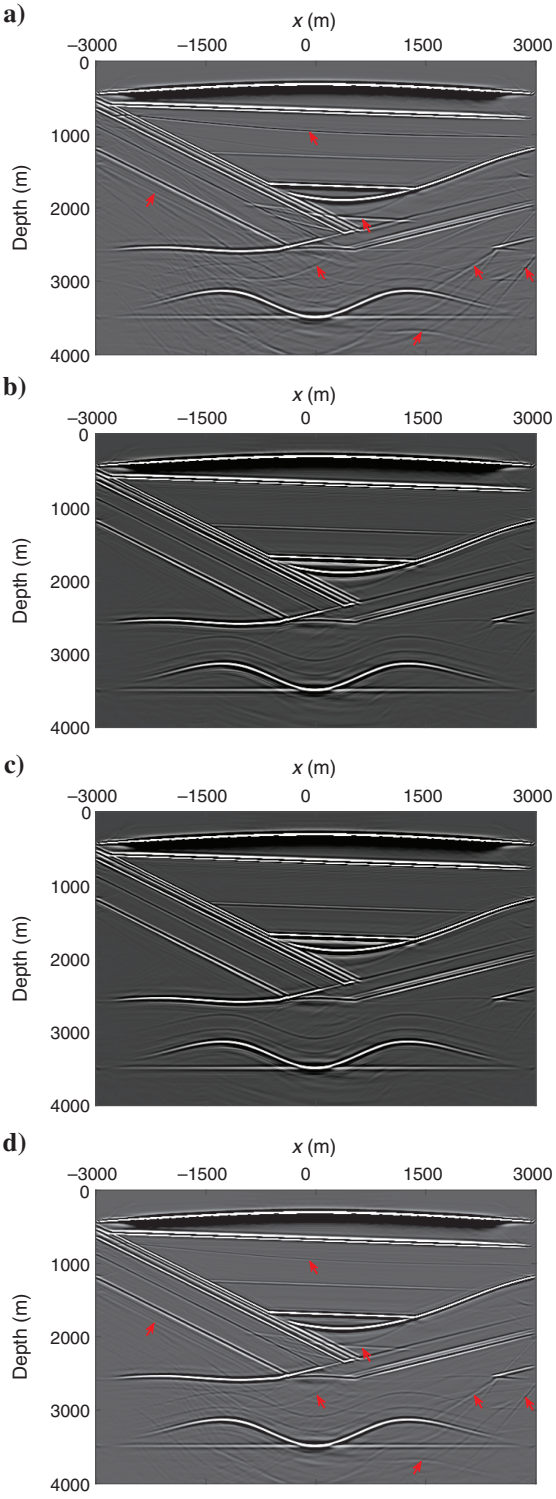

Figure 9. (a) The image retrieved from the computed reflection responses, (b) the image retrieved from the resulting data set of MME, (c) the image retrieved from the resulting data set of T-MME, and (d) the image retrieved from the resulting data set of TKL. The red arrows in (a and d) indicate artifacts due to internal multiple reflections.

strategies behind MME and TKL are different, and the details of MME can be found in Zhang and Staring (2018).

CONCLUSION

We have compared three data-driven internal multiple reflection elimination schemes from theory to performance in numerical examples. Two are derived from Marchenko equations and one from ISS. The theoretical analysis shows that the Marchenko-based schemes are similar to each other but use different truncation operators. This difference implies that the MME scheme only focuses on internal multiple reflection elimination, and the T-MME scheme eliminates internal multiple reflections and compensates for transmission losses in primary reflections. The relation between schemes derived from the coupled Marchenko equations and ISS is also analyzed, showing that the TKL scheme can be understood as the first iteration result of MME. The simple and complex numerical examples show that the Marchenko-based schemes work excellent to eliminate internal multiple reflections, and that the TKL scheme attenuates internal multiple reflections but leaves residuals. These residuals can cause artifacts in the corresponding image.

ACKNOWLEDGMENTS

This work is part of the Open Technology Program with project number 13939, which is financed by The Netherlands Organization for Scientific Research Domain Applied and Engineering Sciences. We would like to thank J. Blanch, S. Singh, and two anonymous reviewers for their valuable suggestions. The research of K. Wapenaar has received funding from the European Research Council (ERC) under the European Union's Horizon 2020 research and innovation program (grant no. 742703).

DATA AND MATERIALS AVAILABILITY

Data associated with this research are available and can be obtained by contacting the corresponding author.

REFERENCES

Berkhout, A. J., and D. J. Verschuur, 1997, Estimation of multiple scattering by iterative inversion — Part 1: Theoretical considerations: Geophysics, **62**, 1586–1595, doi: 10.1190/1.1444261.

Broggini, F., and R. Snieder, 2012, Connection of scattering principles: A visual and mathematical tour: European Journal of Physics, **33**, 593–613, doi: 10.1088/0143-0807/33/3/593.

de Melo, F. X., M. Idris, Z. J. Wu, and C. Kostov, 2014, Cascaded internal multiple attenuation with inverse scattering series: 84th Annual International Meeting, SEG, Expanded Abstracts, 4113–4117, doi: 10.1190/segam2014-0863.1.

Hampson, D., 1986, Inverse velocity stacking for multiple elimination: Canadian Journal of Exploration Geophysicists, **22**, 44–55.

Jakubowicz, H., 1998, Wave equation prediction and removal of interbed multiples: 68th Annual International Meeting, SEG, Expanded Abstracts, 1527–1530, doi: 10.1190/1.1820204.

Löer, K., A. Curtis, and G. A. Meles, 2016, Relating source-receiver interferometry to an inverse-scattering series to derive a new method to estimate internal multiples: Geophysics, **81**, no. 3, Q27–Q40, doi: 10.1190/geo2015-0330.1.

Luo, Y., P. G. Kelamis, S. Huo, G. Sindi, S. Hsu, and A. B. Weglein, 2011, Elimination of land internal multiples based on the inverse scattering series: The Leading Edge, **30**, 884–889, doi: 10.1190/1.3626496.

Matson, K., D. Corrigan, A. Weglein, C. Young, and P. Carvalho, 1999, Inverse scattering internal multiple attenuation: Results from complex synthetic and field data examples: 89th Annual International Meeting, SEG, Expanded Abstracts, 1060–1063, doi: 10.1190/1.1820681.

Meles, G. A., K. Wapenaar, and A. Curtis, 2016, Reconstructing the primary reflections in seismic data by Marchenko redatuming and convolutional

interferometry: Geophysics, **81**, no. 2, Q15–Q26, doi: 10.1190/geo2015-0377.1.
Ravasi, M., 2017, Rayleigh-Marchenko redatuming for target-oriented, true-amplitude imaging: Geophysics, **82**, no. 6, S439–S452, doi: 10.1190/geo2017-0262.1.
Singh, S., R. Snieder, J. Behura, J. van der Neut, K. Wapenaar, and E. Slob, 2015, Marchenko imaging: Imaging with primaries, internal multiples, and free-surface multiples: Geophysics, **80**, no. 5, S165–S174, doi: 10.1190/geo2014-0494.1.
Singh, S., R. Snieder, J. van der Neut, J. Thorbecke, E. Slob, and K. Wapenaar, 2017, Accounting for free-surface multiples in Marchenko imaging: Geophysics, **82**, no. 1, R19–R30, doi: 10.1190/geo2015-0646.1.
Slob, E., K. Wapenaar, F. Broggini, and R. Snieder, 2014, Seismic reflector imaging using internal multiples with Marchenko-type equations: Geophysics, **79**, no. 2, S63–S76, doi: 10.1190/geo2013-0095.1.
Ten Kroode, P. E., 2002, Prediction of internal multiples: Wave Motion, **35**, 315–338, doi: 10.1016/S0165-2125(01)00109-3.
Thorbecke, J., and D. Draganov, 2011, Finite-difference modeling experiments for seismic interferometry: Geophysics, **76**, no. 6, H1–H18, doi: 10.1190/geo2010-0039.1.
van der Neut, J., and K. Wapenaar, 2016, Adaptive overburden elimination with the multidimensional Marchenko equation: Geophysics, **81**, no. 5, T265–T284, doi: 10.1190/geo2016-0024.1.
Verschuur, D., A. Berkhout, and K. Wapenaar, 1992, Adaptive surface-related multiple elimination: Geophysics, **57**, 1166–1177, doi: 10.1190/1.1443330.
Wapenaar, K., J. Thorbecke, J. van der Neut, F. Broggini, E. Slob, and R. Snieder, 2014, Marchenko imaging: Geophysics, **79**, no. 3, WA39–WA57, doi: 10.1190/geo2013-0302.1.
Weglein, A. B., F. A. Gasparotto, P. M. Carvalho, and R. H. Stolt, 1997, An inverse scattering series method for attenuating multiples in seismic reflection data: Geophysics, **62**, 1975–1989, doi: 10.1190/1.1444298.
Zhang, L., and E. Slob, 2019, Free-surface and internal multiple elimination in one step without adaptive subtraction: Geophysics, **84**, no. 1, A7–A11, doi: 10.1190/geo2018-0548.1.
Zhang, L., E. Slob, J. van der Neut, and K. Wapenaar, 2018, Artifact-free reverse time migration: Geophysics, **83**, no. 5, A65–A68, doi: 10.1190/geo2017-0795.1.
Zhang, L., and M. Staring, 2018, Marchenko scheme based internal multiple reflection elimination in acoustic wavefield: Journal of Applied Geophysics, **159**, 429–433, doi: 10.1016/j.jappgeo.2018.09.024.
Zhang, L., J. Thorbecke, K. Wapenaar, and E. Slob, 2019, Transmission compensated primary reflection retrieval in the data domain and consequences for imaging: Geophysics, **84**, no. 4, Q27–Q36, doi: 10.1190/geo2018-0340.1.